Solar Energy Materials & Solar Cells 107 (2012) 381–389

Contents lists available at SciVerse ScienceDirect

Solar Energy Materials & Solar Cells

journal homepage: www.elsevier.com/locate/solmat

Local efficiency analysis of solar cells based on lock-in thermography

Otwin Breitenstein *

Max Planck Institute of Microstructure Physics, Weinberg 2, D-06120 Halle, Germany

ARTICLE INFO

Article history:
Received 15 May 2012
Received in revised form
18 July 2012
Accepted 18 July 2012
Available online 10 August 2012

Keywords:
I–V characteristics
Local analysis
Lock-in thermography
Modeling
Efficiency prediction

ABSTRACT

By evaluating four lock-in thermography images of a solar cell taken at four different biases and an independently measured series resistance image, images of all local two-diode parameters are obtained. Assuming the local validity of the two-diode model, this information enables the construction of local and global dark and illuminated characteristics and of realistic images of local solar cell parameters like efficiency, fill factor, and open circuit voltage with a good spatial resolution. Within this procedure, an injection-dependent lifetime may be regarded by assuming an ideality factor larger than unity for the diffusion current. The possibilities and limitations of this approach are discussed and selected results on a typical industrial multicrystalline cell are introduced. The proposed procedure is a valuable tool for judging which local defects are especially harmful for degrading the fill factor or the open circuit voltage, respectively, and extrapolating the properties of a cell where certain types of defects are excluded. A general limitation of this approach is that it assumes an individual but constant series resistance to each pixel, which neglects the distributed character of the series resistance.

1. Introduction

Local inhomogeneities in solar cells are strongly affecting their efficiency. This holds particularly for inhomogeneities of the dark current–voltage (*I–V*) characteristic, which is a measure of the recombination properties in the device and is influenced by material properties and technological limitations. Sites of locally increased dark current density are traditionally called "shunts" and were originally expected to be generally ohmic. However, it has been found very early that many of these shunts show a non-linear (diode-like) *I–V* characteristic [1,2]. In any case, each internally flowing leakage current represents a current loss and degrades the fill factor (*FF*) and/or the open circuit voltage V_{oc} of a solar cell and must therefore be evaluated. Lock-in thermography performed in the dark (DLIT [3]) is the technique of choice to detect and evaluate such leakage currents, since it directly and quantitatively images the locally dissipated power density in a solar cell. It is usual to describe global and local *I–V* characteristics of solar cells by the two-diode model, attributing the dark current to three contributions, namely the "diffusion current" being characterized by an ideality factor of unity and a saturation current density J_{01}, the (depletion region) "recombination current" being characterized by a saturation current density J_{02} and an ideality factor n_2 (often assumed to be two), and an ohmic "shunt current" characterized by a parallel resistance R_p, which is usually expressed as an area-related resistance in units of $\Omega\,cm^2$ [4]. All these current contributions are defined as a function of the local voltage V_{loc}, which differs from the applied bias voltage V_B by the voltage drop across the series resistance R_s. If the minority carrier lifetime in the material is injection-dependent, the ideality factor of the diffusion current may be larger than unity [5]. If the depletion recombination occurs via extended defects with a high concentration of recombination centers crossing the *p–n* junction, as it may happen in the edge region or at scratches, the ideality factor n_2 of the recombination current may be significantly larger than two [6]. The first attempt to construct local dark and illuminated *I–V* characteristics from LIT images dates back to 1998 [7]. However, the method introduced there was not practicable for general use yet. In particular, it did not allow one to image local solar cell parameters. In an earlier publication [8] it was described that, if an image of the local series resistance R_s is available, images of all four two-diode parameters J_{01}, J_{02}, n_2, and R_p (resp. its inverse, the ohmic conductivity G_p in units of S/cm^2) may be obtained by evaluating four DLIT images, three of them taken at three different forward biases and one taken at a low reverse bias. An iterative procedure managing this local parameter fit was described and implemented in a code called "Local *I–V*", for details of this procedure see [8]. The decisive limitation of this procedure was that it was only able to simulate dark characteristics of the local diode without considering the local series resistance R_s. This series resistance was used for correctly calculating the two-diode parameters, but "Local *I–V*" was not able to display realistic local efficiency or fill factor images. This limitation was due to the fact

* Tel.: +49 345 5582740; fax: +49 345 5511223.
E-mail address: breiten@mpi-halle.mpg.de

0927-0248/$ - see front matter © 2012 Elsevier B.V. All rights reserved.
http://dx.doi.org/10.1016/j.solmat.2012.07.019

that, within the two-diode model, the *I–V* characteristic regarding R_s is only given implicitly. Also illuminated characteristics were not considered yet in "Local *I–V*".

In this contribution a decisive extension of the "Local *I–V*" procedure will be described, which overcomes these limitations and thus enables, among others, the simulation of realistic images of local solar cell parameters, like the local efficiency $\eta(x,y)$, the local fill factor $FF(x,y)$, and the local open circuit voltage $V_{oc}(x,y)$. Note that these local parameters for a certain position (x,y) are actually only "hypothetical" parameters describing the local efficiency potential. They only hold if a whole homogeneous solar cell would have the electronic properties of this very position (x,y). In the usual reality of an inhomogeneous cell, the parallel connection of all local regions leads to an averaged value of the cell parameters, which makes it impossible to measure them locally. Mechanically dividing a cell into small sub-cells is destructive and inevitable creates additional leakage currents at the edges of the sub-cells, just as any real solar cell edge is characterized by an edge current [3,6,8]. The goal of the procedure introduced here is to "measure" these local solar cell parameters non-destructively. Actually, the local dark characteristics are fitted to the DLIT measurement, and from these data the illuminated characteristics are simulated, leading to the local solar cell parameters. This enables a detailed local efficiency analysis of inhomogeneous solar cells, including the information which local defects are most dangerous for degrading *FF* and V_{oc}, and what is the efficiency potential of a cell if certain defects were avoided. Of course, this DLIT-based local efficiency analysis is based on several simplifying assumptions, which will be summarized and discussed in the following section. Results of an efficiency analysis of a typical industrial multicrystalline solar cell using two different R_s-data are presented in Section 3 (Results), and the significance of the results and limitations of the procedure are discussed in Section 4 (Discussion).

2. Procedure

The first version of the "Local *I–V*" method was described in detail already in [8], therefore here only its basic principles will be summarized. As outlined in [3], for wafer-based solar cells, the -90° DLIT signal image data $T^{-90^\circ}(x,y)$ (given in any units, e.g., mK) may be converted into a power density image $p(x,y)$ by applying:

$$p(x,y) = \frac{T^{-90^\circ}(x,y)P}{\langle T^{-90^\circ}(x,y)\rangle A} \tag{1}$$

here P is the power dissipated by the cell during the pulse period (voltage times current), A is the cell area, and $\langle T^{-90^\circ}(x,y)\rangle$ is the average value of the -90° signal across the whole solar cell. The evaluation after (1) provides a spatial resolution in the order of one thermal diffusion length, which is about 2 mm for a lock-in frequency of 10 Hz [3]. This formula holds true independent of the accuracy of the temperature reading of the camera and of the local infrared (IR) emissivity (as long as it is homogeneous), since these parameters influence the local and the average -90° signal in the same way. The "Local *I–V*" method relies on the fact that different dark current contributions are characterized by different dependencies of the current on the local voltage across the *p–n* junction. This local voltage may deviate from the bias voltage V_B applied to the cell, since there is a series resistance to each position causing an inevitable voltage drop, depending on the local current density. If this voltage drop would not be considered, the quantitative evaluation would not work correctly. Since the area-related series resistance $R_s(x,y)$ (given in units of $\Omega\,cm^2$) may be distributed inhomogeneous, the "Local *I–V*" procedure needs an R_s-image of the investigated cell as an input. This image may be measured e.g., by photoluminescence (PL) or electroluminescence (EL) imaging [9,10] or by applying the so-called RESI method, which is a combination of EL and DLIT imaging [11]. Alternatively, if the evaluation is made at relatively low voltages, where a low current is flowing and the voltage drop is weak, the series resistance also may be assumed to be locally constant. From the locally dissipated power density measured by DLIT, the applied bias V, and the known local value of R_s the local voltage across the junction V_{loc} and the locally flowing current density $J(V_{loc})$ may be calculated, as it was described in [8]. It is well-known and generally accepted that, assuming a constant minority carrier lifetime in the material, the local dark *J–V* characteristic may be described in each position by the so-called two-diode model described by [4]:

$$J(V_{loc}) = J_{01}\left(\exp\frac{eV_{loc}}{kT}-1\right)+J_{02}\left(\exp\frac{eV_{loc}}{n_2kT}-1\right)+\frac{V_{loc}}{R_p} = J_{diff}(V_{loc}) + J_{rec}(V_{loc})+J_{shunt}(V_{loc}) \tag{2}$$

J_{01} is the saturation current density of the diffusion current J_{diff}, J_{02} is the saturation current density and n_2 the ideality factor of the (depletion region) recombination current J_{rec}, R_p is the parallel resistance governing the shunt current J_{shunt}, and kT/e is the thermal voltage being 25.69 mV at 25 °C. The local diode parameters must be determined for each position (x,y) separately. The extraction of these local parameters from DLIT images is the goal of the "Local *I–V*" procedure. This problem is solved by evaluating the results of four DLIT images taken at four different biases V_1, V_2, V_3, and V_{rev}, three of them under forward and one under reverse bias. First, all DLIT images are converted into power density images by applying (1). Then the four unknown diode parameters J_{01}, J_{02}, n_2, and R_p are obtained for each position by applying a special iterative procedure described in [8], which fits in each position (x,y) the four $J(V_{loc})$ data pairs of the four voltages, where the DLIT images have been taken, to the two-diode model (4). While the previous "Local *I–V*" procedure has neglected the influence of the 2nd diode on the reverse current, this influence, which may be measurable for very large ideality factors, is regarded in the new procedure "Local *I–V* 2". Thus, this new procedure also includes the ohmic conductivity $G_p = 1/R_p$ in the iteration by including a forth equation in the iteration loop, fitting the ohmic and the recombination current to the measured reverse current. Therefore "Local *I–V* 2" allows a correct fitting of all four voltage points of characteristics having ideality factors up to 50.

Once the four diode parameters are calculated for each position (x,y), and $R_s(x,y)$ is known, the solar cell is completely locally characterized. Then the dark *I–V* characteristics of the local diodes (without regarding R_s) may be calculated for each single position (x,y) or as an average over a certain selected region of the cell by applying (2). This kind of characteristic, without the influence of the series resistance, is in the PV community often called "suns-V_{oc}" characteristic [12]. For a whole solar cell, it can be obtained by measuring the open circuit voltage V_{oc} as a function of the illumination intensity measured in units of "suns" (one "sun" equals 1000 W/m^2 at AM 1.5). From the suns-V_{oc} characteristic the "illuminated suns-V_{oc}" characteristic may be obtained by applying the superposition principle, indicating that the illuminated characteristic equals the dark characteristic shifted in current-direction by the short circuit current density J_{sc}:

$$J_{illum}(V_{loc}) = J_{dark}(V_{loc}) - J_{sc} \tag{3}$$

This principle holds because the photo-induced current is independent of the voltage, in contrast to the dark current. Under short circuit condition ($V=0$), the dark current is zero and only

the photo-induced current J_{sc} flows. If the dark current is defined to be positive, the illuminated current is negative, since it is a reverse current. Nevertheless it is usual to display also illuminated characteristics as a positive current, as it will be done also in the following.

If the local series resistance has to be regarded in I–V characteristics, which corresponds to the calculation of "real" I–V characteristics, the current values cannot be expressed analytically anymore. Note that the local current density J also influences V_{loc} in (2). Nevertheless, for any value of V_{loc} the current density may be calculated after (2), from which, knowing R_s, the applied bias voltage V_B may be calculated. In the new software code "Local I–V 2", where this procedure is implemented, this calculation is performed in the dark and under illumination for a representative number of V_{loc}-values, and the resulting J–V_B data pairs (which are not equidistant in V_B) are re-sampled and stored for any position (x,y) in a 3-dimensional temporary lookup-table to obtain the local current values of any arbitrary V_B. The "Local I–V 2" software, like the former version, allows one to display images of the two-diode parameters, of the total dark current, or of any of the three current components J_{diff}, J_{rec}, or J_{shunt} at any of the three forward biases. Moreover, it now also calculates images of local cell parameters, like the local open circuit voltage V_{oc} (which is, of course, independent of R_s), the local fill factor FF, and the local efficiency η, see below. The local short circuit current density $J_{sc}(x,y)$ may be either assumed to be homogeneous or may be loaded as a J_{sc}-image. Such an image for AM 1.5 may either be measured by evaluating spectrally resolved light beam-induced current (LBIC) measurements (see [13]) or eventually by properly evaluating local bulk recombination properties obtained from EL or PL images (see [9,10]). Based on the illuminated suns-V_{oc} characteristics calculated by (3), images of the so-called "pseudo fill factor" pFF and the "suns efficiency" η_{suns} are also calculated, which both do not regard the local series resistance. Also images of the effective ideality factor and of the effective "suns-V_{oc}" ideality factor (without the influence of R_s) are calculated between V_1 and V_2 and between V_2 and V_3, respectively. Finally and most importantly, by using the R_s-corrected local I–V data stored in the lookup table, the "Local I–V 2" software simulates also "real" local characteristics considering the local R_s, either in the dark or illuminated, for any position (x,y) or for a selected region. Based on these local illuminated characteristics, the images of the local V_{oc}, FF, and η are calculated. It was already mentioned that these efficiency parameter images only describe the local efficiency potential. They are all calculated for the individual maximum power point (mpp) in each position. Therefore, for a given global mpp-voltage of the whole cell, also images of the local voltage, current density, fill factor, and the generated power density at this global mpp are calculated. These data may be compared with local efficiency imaging data obtained e.g., by illuminated LIT investigations [14] or photoluminescence imaging [15]. An important option is to calculate local dark and illuminated I–V curves (for any chosen illumination intensity), both of single positions and of selected extended regions. In the latter case the pixel currents are summed up over the selected region. Since this region may also be the whole cell, the procedure enables the simulation of "suns-V_{oc}" characteristics (hence dark or illuminated characteristics of the local diode, local voltages averaged) or "real" I–V characteristics of whole solar cells, based on their local analysis. The "Local I–V 2" code is available at [16] or via the author.

The approximations underlying this procedure are the following:

(1) It assumes the validity of the two-diode model for any position. Hence it assumes that the superposition principle holds (the photocurrent is independent of the bias, and the dark current flows unchanged also under illumination), and that the ideality factors n_1 and n_2 of J_{01} and J_{02}, respectively, are independent of the local voltage. The value of n_1 may be entered as a parameter holding everywhere, whereas n_2 may either be assumed to be two or may be taken as a variable, which is fitted to the experimental data. Note that there are known departures from the superposition principle. Based on PC1D-simulations, Robinson et al. [17] have pointed to two common departures from the superposition principle, from which departure 2 is most distinct for strong recombination in the bulk or at the backside. The reason for this departure is that, under illumination at zero Volt bias (short circuit), the minority carrier concentration and thus the recombination rate in the bulk is significantly higher than at zero bias in the dark. This effect is proportional to the current density and acts on the illuminated characteristic like an additional parallel conductivity or a recombination current. Thus, it mainly leads to an additional reduction of the fill factor. Note that these minority carriers are the reason why for PL image evaluation always the PL image under short circuit has to be subtracted [9]. It can be assumed that the remaining weak deviation between our simulated and measured illuminated characteristic shown below is at least partly due to this effect, since our fill factors appear generally slightly too large. Moreover, since there may be serious departures from the superposition principle for certain types of thin film solar cells, the procedure described here is less appropriate for such cells.

(2) The procedure assumes that each pixel is characterized by an own area-related current-independent series resistance R_s, which is conventionally defined as the local voltage drop divided by the locally flowing current density [9–11]. Though this concept is widespread, it is actually wrong, since all currents flowing horizontally in the grid lines or in the emitter are leading to a distributed series resistance. This means that the local I–V characteristics of all diode positions along a horizontal current path contribute to the voltage drop across this path. In this way, the characteristics of different regions interfere with each other; the voltage drop in one position depends also on the characteristic in another position in the same current path. This is due to the fact that, depending on the magnitude of the current in the high current regime, the current paths may be different. For the whole cell, if the local diode properties are essentially homogeneous, a distributed series resistance may be described as a current-dependent lumped R_s [18]. However, since in an inhomogeneous cell different regions show different I–V characteristics, the mentioned interference between different regions prevents that even a variable local R_s may describe the voltage drop in a certain position under all biasing and illumination conditions. This does not mean that the conventional definition of a constant local R_s is useless. For a certain operation condition of the cell (dark or illuminated, at a certain current level) it correctly describes the local voltage in the device. Thus, for the procedure described here it is advisable to use a series resistance image measured under the condition of the highest forward bias of the DLIT images used in the analysis, where the series resistance has the strongest effect.

(3) The procedure assumes that the local DLIT signal is proportional to the local product of voltage times current density. This proportionality is based on the energy conservation law, which holds for the whole cell but not necessarily locally. Note that also the Peltier effect, which does not dissipate power but transports latent heat over certain distances, influences the local temperature modulation. If a forward current flows in the dark, there is Peltier cooling at the two metal-semiconductor contacts, there is a strong Peltier cooling at the p–n junction, and some part of the recombination

energy represents the corresponding Peltier heating; the sum of all Peltier effects being zero [3,19,20]. If any horizontal current is flowing in the cell, the Peltier heating or cooling may lead to local thermal signals different to that expected by the energy conservation law. This law can only be used for interpretation of DLIT signals if there is essentially vertical current flow in the region under investigation, where all Peltier heat flows cancel each other [3,19]. Since the spatial resolution of the DLIT results used here is about 2 mm, which is large compared to the cell thickness of 0.2 mm, this condition is met here. However, if the spatial resolution should be further improved, e.g., by working at a considerably higher lock-in frequency or by applying spatial deconvolution [3], care must be taken for the disturbing influence of Peltier signals.

(4) The procedure only evaluates the heat dissipation at the local diode and neglects the heat dissipation at the series resistances. This leads to negligible errors as long as the voltage drop at R_s is low compared to the bias voltage. It has been shown in [8] that, even if this is not the case, the results still remain reasonable. Nevertheless, since also the DLIT signal in high-R_s region is weak and its noise level is high, the procedure described here works most reliably with solar cells not having serious R_s problems.

(5) This procedure assumes a homogeneous infrared (IR) emissivity and a meaningful DLIT signal across the whole cell. In positions, where this is not the case (bare cell, leading to low emissivity at Ag grid lines and in the edge region due to the missing Al back contact there, shadowing of the bus bars by current leads), the dark current may be underestimated. While this effect is negligible for the narrow grid lines, as long as whole large solar cells are investigated, it is not negligible in the bus bar regions. In "Local *I–V* 2", the bus bar regions may be marked as a "bad pixel" regions, where their DLIT input data values are replaced by the average values of their surrounding.

3. Results

All results shown here are obtained on a typical 156×156 mm^2 sized industrially processed multicrystalline solar cell in standard technology (iso-textured, $POCl_3$-diffused, screen-printed metallization, full-area Al back contact). The measured and simulated cell parameters are summarized in Table 1. This cell, which shows a relatively high R_p of 11.6 kΩ cm^2 (no ohmic shunt problems), was already characterized in detail in [21].

3.1. Measurement conditions

All measurements were made at a cell temperature of 25 °C. First it had to be decided under which conditions the DLIT images are measured and which type of R_s image should be used.

Table 1
Cell data as provided by the producer, as monochromatically measured (850 nm), as simulated using PL-R_s data, as simulated using RESI-R_s data, and as simulated using RESI-R_s data and assuming $n_2=2$.

	Producer data	850 nm meas.	PL-R_s sim.	RESI-R_s sim.	RESI, $n_2=2$
J_{sc} [mA/cm^2]	31.8	31.8	31.8	31.8	31.8
V_{oc} [mV]	625	624	623	625	625
FF [%]	76.5	77.6	77.5	78.0	78.1
η [%]	15.2	15.4	15.4	15.5	15.5

The signal-to-noise ratio of any DLIT image strongly depends on the lock-in frequency, the acquisition time, and on the signal amplitude, hence on the power dissipated by the cell during the measurement. For the DLIT images shown here a lock-in frequency of 10 Hz and an acquisition time of 1 h per image has been selected. The cell was imaged barely and multi-point contacting and 4-point probing was applied. Since there is no Al back contact in the edge region, which contributes to the IR emissivity, and the bus bar region is shadowed here by the current leads, current contributions from these two regions may be somewhat underestimated. The general rule for the application of "Local *I–V*" is: the signal-to-noise ratio (SNR) of the results is the better, the higher the currents during the measurements and the higher the voltage differences between them. On the other hand, the lower the voltages (and currents) of the DLIT measurements is, the less important is the voltage drop at the series resistance. Hence, if no series resistance image is available and a constant series resistance has to be assumed, it is advisable to work with lower currents. Then the error of eventually wrong R_s-values is low, but the SNR of the results is also low. Since here we wanted to compare the influence of different R_s images, it was decided to work with relatively high biases resp. currents. All results shown here are based on four DLIT images taken at 0.5 V (173 mA), 0.55 V (563 mA), 0.60 V (2361 mA), and −1 V (−24 mA). It has been found that the qualitative results of this procedure (e.g., the distinction between diffusion and recombination current) are only little dependent on the selection of the measurement biases. If lower biases are chosen, or if the biases are lying more closely together, the SNR of the results degrades. A significantly higher reverse bias than −1 V should be avoided for excluding any pre-breakdown effects. For improving the SNR, pixel binning of 2×2 was applied, leading for the originally 512×512 pixel images to 256×256 pixel results. Two independently obtained R_s images were used. The first is a PL-based R_s image after Trupke [9] taken close to the maximum power point, which was kindly provided by D. Hinken from ISFH (Hameln) and was shown already in [21]. The second R_s image is a so-called RESI image [11]. Here the local voltage at the highest applied forward bias of $V_3=0.6$ V is measured by evaluating two EL images, one taken at 0.56 V and one taken at 0.6 V by using the "EL-Fit" procedure described in [22]. Alternatively, the local EL-bias at 0.6 V may also be calculated by evaluating a 0.6 V EL image and an EL image at a considerably lower bias as a "scaling image" after [9,10]. The "Local *I–V* 2" procedure allows one to calculate the RESI-R_s image after [11] from such a loaded $V_3(x,y)$ image and the DLIT image of V_3. Note that this is a "dark R_s" image, whereas the PL-R_s image is an "light R_s" image. As it will be discussed in the following section, there are significant local differences between these two R_s images.

3.2. Global characteristics and local diode images

Fig. 1 shows most of the input images used in this investigation. In (a) to (c), instead of the original DLIT images, the current density images scaled in mA/cm^2 calculated by (3) are shown. Qualitatively, these images are indistinguishable from the input DLIT images, apart from their different scaling units (mA/cm^2 vs. mK). This points to the fact that, as long as the series resistance is so low that the local voltage drop is only a few 10 mV see Fig. 1e, the procedure (3) leads to negligible changes of the current density, compared to the usual procedure $J=p/V_B$ without regarding R_s [3]. However, it is important to regard even a weak R_s for calculating the correct local voltage V_{loc}, which may strongly influence the assignment of the current components. Many sites of increased forward current (shunts) are visible in (a) and (b), but only a few of them, which show an ohmic conductivity contribution,

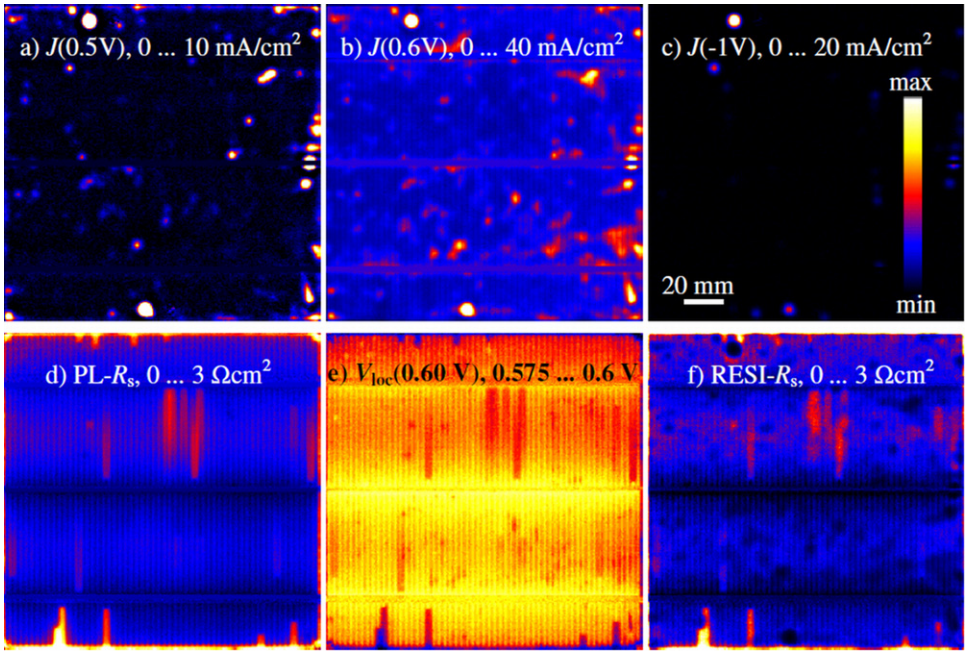

Fig. 1. (a) Current density at 0.5 V, (b) current density at 0.6 V, (c) current density at −1 V, (d) PL-R_s image, (e) local voltage image from EL at 0.60 V, (f) RESI-R_s image. All scaling limits are indicated, the color and scaling bars in (c) hold for all images.

are also visible in (c). The two dominant shunts at the top and at the bottom of the cell appear artificially broadened in this scaling range; in an optimized scaling range they also appear point-like. At 0.5 V there is a low amount of homogeneous current compared to 0.60 V, and at −1 V there is no homogeneous current at all. This confirms earlier findings that the homogeneous current is only due to the diffusion current, which dominates at higher forward bias, and that there is no homogeneous ohmic current [21]. Fig. 1d shows the PL-R_s image, (e) the local voltage image $V_3(x,y)$ obtained from EL image evaluation, and f) the RESI-R_s image, calculated from (b) and (e), in the same scaling as (d). We see that, though (d) and (f) generally show the same features, there are clear differences between the two R_s images. It is obvious that the RESI-R_s image shows local minima in the positions of some local shunts (sites of increased current density at 0.6 V). These sites are partly visible as dark spots in the local bias image (e). This could be expected since, due to the locally increased dark current, there is an additional voltage drop in these positions. The difference between the two R_s images (d) and (f) are mainly due to the different local current distribution in both measurements. While in the PL-R_s measurement the dominant current was the photocurrent, which flows essentially homogeneous, in the RESI-R_s measurement it is the dark current at 0.6 V, which flows very inhomogeneous, see Fig. 1b. While the horizontal current paths under illumination are essentially linear and parallel, first from the emitter area to the grid lines, and then within the grid line to the bus bar, the current to a local shunt may be conducted from all four sides. This leads to a reduced local effective R_s-value in this region, if the series resistance is defined conventionally as the local voltage drop divided by the local current density. Hence, the local minima in the RESI-R_s image are real, and they do not appear under illumination. The difference between Fig. 1d and f indicates a basic limitation of the local R_s concept used here: there is no universal local R_s-distribution characterizing the cell under all conditions (dark and illuminated, different current levels). Note that there may be also still some systematic errors in the RESI-R_s image, coming from the fact that the EL-based calculation of $V_3(x,y)$ is generally assuming a diode ideality factor of unity. If there are J_{02}-type or ohmic shunts in the cell, they are interpreted in the evaluation as low lifetime regions, which may lead to some inaccuracy of the V_3-estimation in such regions.

In the following simulations a homogeneous short circuit current density equal to the value provided by the producer of the cell for AM 1.5 was assumed. In reality J_{sc} should be higher than this average in defect-free regions and lower in defect regions. Thus, in the present evaluation the maximum efficiency limit is probably still underestimated. Fig. 2 shows the measured dark and illuminated I–V characteristics, together with the global characteristics simulated by "Local I–V 2" by summing up over all image pixels, using the PL-R_s and the RESI-R_s data from Fig. 1d and f, respectively, and also assuming $n_2=2$. Since the flasher-based I–V data of this cell were not available and there was no access to a cell tester, we measured the illuminated characteristic under monochromatic illumination. The cell was homogeneously illuminated with 850 nm light and the intensity was adjusted to match the $J_{sc}=31.8$ mA/cm^2 given by the cell producer. As Table 1 shows, the cell data measured in this way match the flasher-based I–V data provided by producer quite well. Only the fill factor measured by us is significantly larger, which may be due to a lower influence of the departure from the superposition principle described in [17] in our case. Note that in this type of solar cells the backside recombination at the Al contact considerably contributes to the effective bulk recombination, which has a stronger influence for AM 1.5 than for 850 nm illumination. In Fig. 2a the measured dark characteristic is matched also very well by the simulations using both R_s data. It can be expected that, especially for low currents, the choice of R_s does not play a significant role. In spite of the fact that the DLIT measurements were lying quite closely together (see data points in a), the fit of the dark characteristic is very good down to 0.2 V. This supports our assumption that the ideality factor of local non-linear (recombination-type) shunts is rather independent from the bias. If an ideality factor of the recombination current of $n_2=2$ is assumed, the fit below 0.5 V becomes considerably worse, but there is no influence in the high current regime. Above the highest current used for the DLIT measurements, all simulated dark characteristics indicate a series resistance assumed to be too

high. This deviation is a result of the conventional (area-related) definition of R_s, which does not take into account its distributed character. In reality, the effective (lumped) dark series resistance further decreases in the high-current regime above 0.6 V [18]. Fig. 2b shows the measured and simulated illuminated characteristics, the dots are the maximum power points. As Table 1 shows, the efficiencies differ only by 0.1% and the V_{oc} by 2 mV from the measured ones. In particular, the maximum power points are lying closely together. Therefore only the region around the maximum power points are displayed in Fig. 2b, which allows a distinction between the different results. Only slight deviations between the measurement and the different simulations are visible. In the illuminated characteristics (b), the PL-R_s-based simulation is lying a little closer to the measured curve, but the difference to the RESI-based simulations is weak. The simulations for variable n_2 and assuming $n_2=2$ are lying very close to each other, the only difference is in the low-voltage range, as could be expected. Hence, for the simulation of illuminated characteristics the assumption of $n_2=2$ obviously does not lead to significant errors, just as for the dark characteristics at the maximum power point and above.

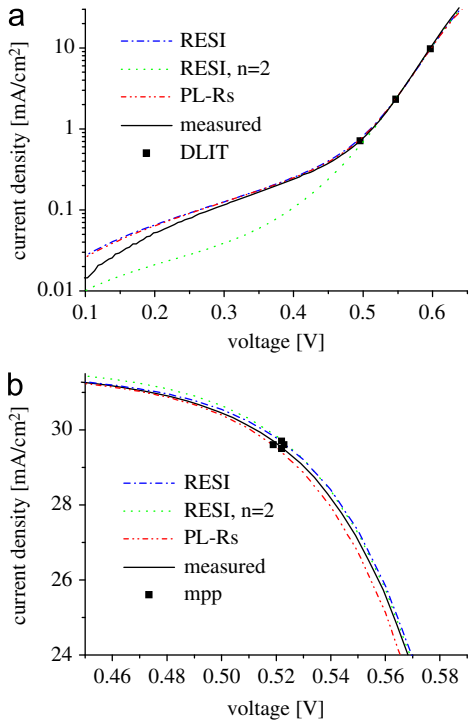

Fig. 2. (a) Measured and simulated dark characteristics (dots: DLIT measure points), (b) measured and simulated illuminated characteristics (detail, dots: maximum power points, see text).

Though there are only little differences between the two R_s data sets in the global analyses, there are clear differences in the local analysis. The accuracy of the modeling of certain local shunt currents is better if the RESI-R_s data are used. By using the PL-R_s data, the series resistance in most shunt positions is clearly overestimated. This results in too large voltage corrections for the high-current measure points in shunt position, leading to a physically unlikely steep local characteristic there (ideality factor significantly smaller than unity). Therefore, in the following we will generally use the RESI-R_s data with variable n_2 for our simulations. "Local I–V 2" allows the limitation of the allowed range of n_2 (as well as of all other fitting parameters), here a range between 2 and 20 has been chosen. Choosing n_2 values well below 2 is not recommended, since then the procedure may have problems to separate the diffusion and the recombination current contributions from each other. Values above 20 are probably physically irrelevant. Fig. 3 shows a collection of images resulting from the "Local I–V 2" evaluation of the data shown in Fig. 1. The J_{01}-image closely correlates to the EL image (not shown here; high J_{01}-values in positions of low EL signal), as it had been shown already in [21]. If n_2 is taken as a variable, the J_{02}-data range over many orders of magnitude. Therefore, in Fig. 3b $\log(J_{02})$ is shown from 10^{-8} to 10^{-2} A/cm^2. This J_{02}-image closely correlates with the n_2-image (Fig. 3c). This agrees with the theoretical expectation that a high local concentration of recombination centers

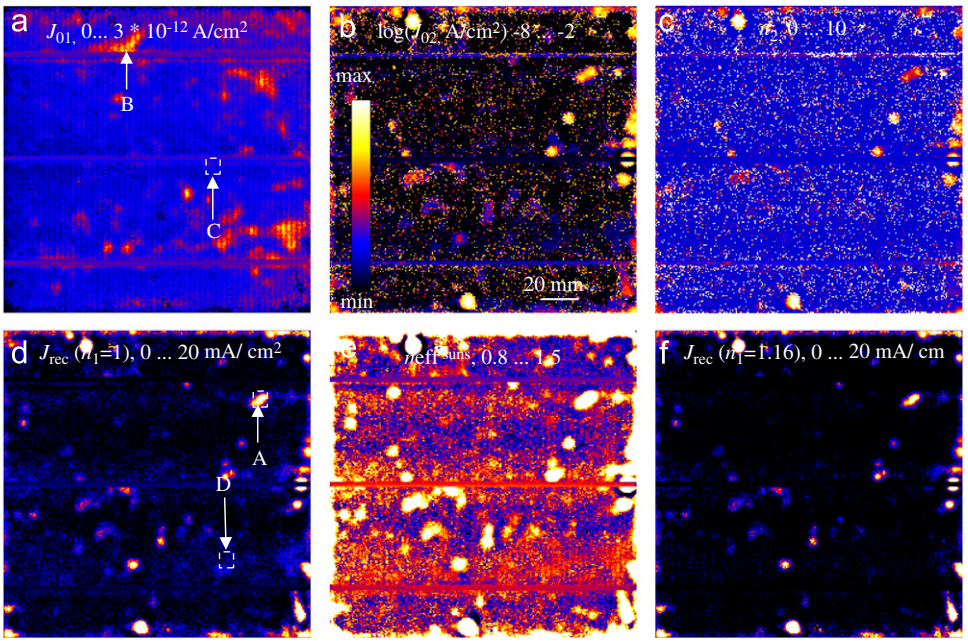

Fig. 3. Images of (a) J_{01}, (b) J_{02} (variable n_2, logarithmically displayed from 10^{-8} to 10^{-2} A/cm^2), (c) n_2, (d) J_{rec} (0.6 V, variable n_2, $n_1=1$ assumed (e) "suns-V_{oc}" effective ideality factor, measured between 0.55 and 0.6 V, (f) J_{rec} (0.6 V, variable n_2, $n_1=1.16$ assumed). All scaling limits are indicated, the color and scaling bars in (b) hold for all images.

crossing the p–n junction leads to pronounced multi-level recombination, which is responsible for the high ideality factors [6]. The strong noise in the n_2-image is due to the fact that in most of the area the recombination current is very small. Since the J_{02}-data are strongly influenced by the of the n_2-data, very often the approximation $n_2=2$ is made, even if the dark characteristic indicates $n_2>2$, since only then the J_{02}-image is physically meaningful: it is proportional to the locally flowing recombination current density. This recombination current component at 0.6 V can also be displayed by "Local I–V 2" for variable n_2, the result is shown for 0.6 V in Fig. 3d. This image looks quite similar to the measured current density at 0.5 V in Fig. 1a, where at 0.5 V the recombination current contribution should dominate. However, there are also significant currents in Fig. 3d in positions where J_{01} see Fig. 3a shows local maxima (e.g., in region D in Fig. 3d. This points to the possibility that the procedure has not completely separated J_{01}- and J_{02}-contributions here. Note that the separation of these two current contributions depends basically on two parameters: (1) on the assumed value of R_s and (2) on the assumed value of n_1. R_s influences the amount of the voltage correction: the larger R_s, the smaller the effective ideality factor, the higher the amount of current attributed to J_{01}, and vice versa. Thus, R_s-values chosen too low would lead to the attribution of some of the diffusion current to the recombination current. As mentioned above, a carrier-dependent saturation of recombination centers may lead to an increase of the ideality factor of the diffusion current n_1 [5]. If n_1 is larger than unity but $n_1=1$ is assumed, some part of the diffusion current is also attributed as a recombination current. As mentioned above, "Local I–V 2" automatically calculates images of the "effective ideality factor" between V_1 and V_2 and between V_2 and V_3, respectively, which is the inverse of the slope of the logarithmic characteristic between these points. Here in each position (x,y) the dominant current contribution governs the value of this magnitude. For high currents it is well known that the effective ideality factor is influenced (enlarged) by the series resistance. Therefore "Local I–V 2" also calculates images of the "suns-V_{oc}" effective ideality factors, where the influence of R_s is compensated. Fig. 3e shows this image for the voltage range 0.55 to 0.6 V. Indeed, this image is not influenced by the inhomogeneities of R_s, as the conventional effective ideality factor image indeed is. The scaling range of this image spans from 0.8 to 1.5, hence all regions where the recombination current dominates appear white. This sensitive scaling was chosen for showing that in crystal defect regions, where the diffusion current (Fig. 3a) is maximum, also the effective ideality factor is slightly increased over unity (blue in the on-line color version). In these defect regions, n^{eff}-values of 1.16 and above are observed, whereas in most "good crystal quality" regions n_{eff}-values very close to unity appear. Therefore in Fig. 3f a J_{rec} image assuming $n_1=1.16$ is displayed. This image looks already much closer to Fig. 1a), hence probably the assumption $n_1=1.16$ is somewhat more realistic than $n_1=1$, at least for the crystal defect regions. By this measure the diffusion current image remains qualitatively unchanged compared to Fig. 3a. Note, however, that by assuming $n_1>1$ the numerical values of J_{01} are not comparable with that assuming $n_1=1$ anymore, just as it is for J_{02}-values and $n_2=2$. Also any inaccuracy of the R_s image may lead to deviations of the local n^{eff}-values, note the above mentioned limited validity of the local R_s concept applied here. This probably explains the generally higher n^{eff}-values close to the bus bars. Moreover, in the defect regions also a weak homogeneous recombination current may be expected, which also would increase n^{eff} in these regions. Therefore, and since there is obviously no generally valid value of n_1, the following evaluations are performed again by assuming $n_1=1$. It has been tested that assuming $n_1>1$ would not lead to significant changes in these results. By comparing Fig. 3a and d (resp. f) it can be observed that there are distinct J_{01}-shunts (regions of high diffusion current) and J_{02}-shunts (region of high recombination current), which show only a weak correlation to each other. While J_{02}-shunts are mostly lying within regions of increased J_{01}, there are also pure J_{01}-shunts, where no measurable J_{02} flows. For example, site A is a typical $J_{02}+J_{01}$-shunt, site B is a typical J_{01}-shunt, and site C is a high crystal quality region. We will refer to these sites in the discussion of the local characteristics and solar cell parameter images in the following section.

3.3. Local characteristics and cell parameter images

Fig. 4a, b, and c show the dark and illuminated characteristics of regions A, B, and C. The local solar cell parameters of these regions are indicated in the caption. For the dark characteristics the suns-V_{oc} characteristics are shown here, since only these can easily be split into the diffusion and recombination current contributions (note that R_s only acts on the total current and not on its constituents). The ohmic current contributions in these regions are negligible and not shown. It is clearly visible that in region A both *FF* and V_{oc} is degraded, leading to a strong reduction of the efficiency, whereas in region B mostly V_{oc} is degraded. Region C marks the efficiency potential of this cell of 16.4% at $V_{oc}=632$ mV, which would hold if all local defects were absent and R_s were as low as in this region. Note that, for a more realistic J_{sc}-distribution, this potential would be even higher. In Fig. 4d the dependence of the efficiency on illumination intensity is plotted for regions A, B, and C, and for the whole cell. As expected, this dependence is especially strong for region A and weakest for region C.

In Fig. 5 various local cell parameters are shown, which are obtained assuming full illumination intensity ($J_{sc}=31.8$ mA/cm^2), except of the V_{oc}-distribution d), where an intensity equivalent to 0.2 suns ($J_{sc}=6.36$ mA/cm^2) was assumed. By comparing these data with the diode parameter data in Fig. 3 (especially the distribution of the diffusion current a) and the recombination current f), it is visible that V_{oc} at 1 sun (Fig. 5a) is mainly influenced by local maxima of the diffusion current (Fig. 3a) and less by the recombination current distribution (Fig. 3f). The opposite holds for the distribution of the fill factor (Fig. 5b), which is stronger influenced by maxima of the recombination current (Fig. 3f). All local efficiency variations (Fig. 5c) may be explained by variations of V_{oc} (Fig. 5a) or *FF* (Fig. 5b, which is influenced by R_s, Fig. 1e), since here a homogeneous J_{sc} has been assumed. On the other hand, at a reduced illumination intensity of 0.2 suns, also V_{oc} (Fig. 5d) is strongly influenced by sites of high recombination current (Fig. 3f). At this intensity V_{oc} is close to the mpp at full illumination intensity, where the *FF* at 1 sun is measured. This shows that the recombination current has a stronger influence on the characteristic at mpp than at V_{oc}, which is also visible in the FF image at 1 sun in Fig. 5b. Also the *FF* and efficiency images measured at 0.2 suns (not shown here) showed a stronger degradation in positions of J_{02} shunts than for 1 sun. This shows that these defects affect the efficiency much stronger at reduced illumination intensity, which also holds for ohmic shunts. This is also nicely shown in Fig. 4d, where defect A shows the strongest degradation of the efficiency with reducing intensity. The pseudo-*FF* and the suns-efficiency images Fig. 5e and f display the local diode properties without the influence of the local series resistance. Indeed, the inhomogeneities of R_s (Fig. 1d and f) are not visible in these images anymore, just as in the V_{oc}-images (Fig. 5a and d). This points to the fact that the procedure of Eq. (3) to regard R_s is obviously correctly working, which has been shown for even stronger R_s-variations already in [8].

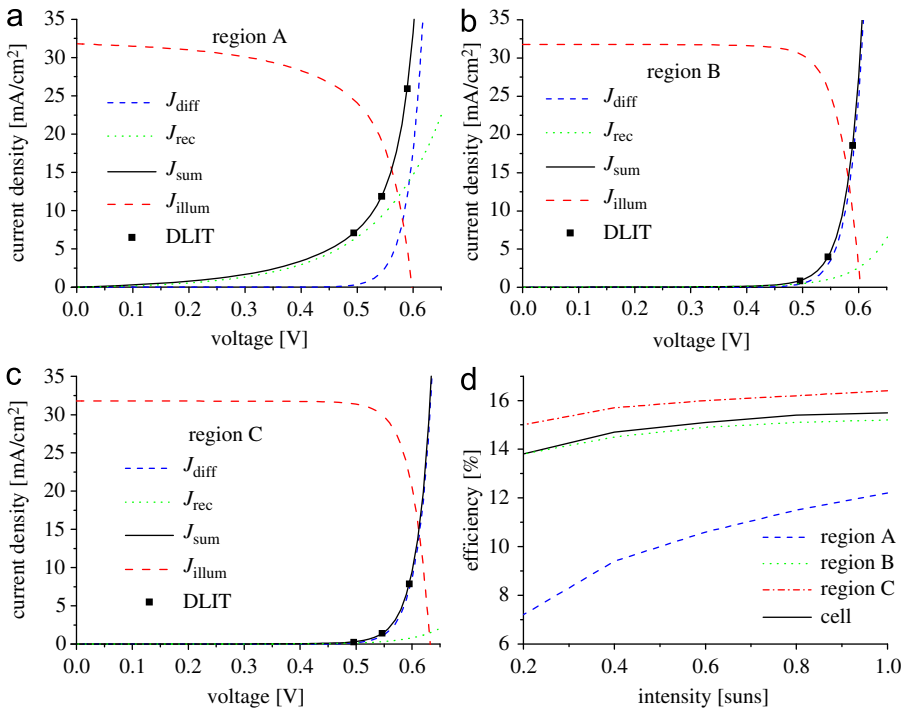

Fig. 4. Suns-V_{oc} characteristics, split into diffusion- and recombination current, and illuminated characteristics of (a) region A (V_{oc}=598 mV, FF=64.0%, η=12.2%), (b) region B (V_{oc}=604 mV, FF=79.4%, η=15.2%), and (c) region C (V_{oc}=632 mV, FF=81.5%, η=16.4%). (d) Dependence of the efficiency on illumination intensity for regions A, B, and C, and for the whole cell.

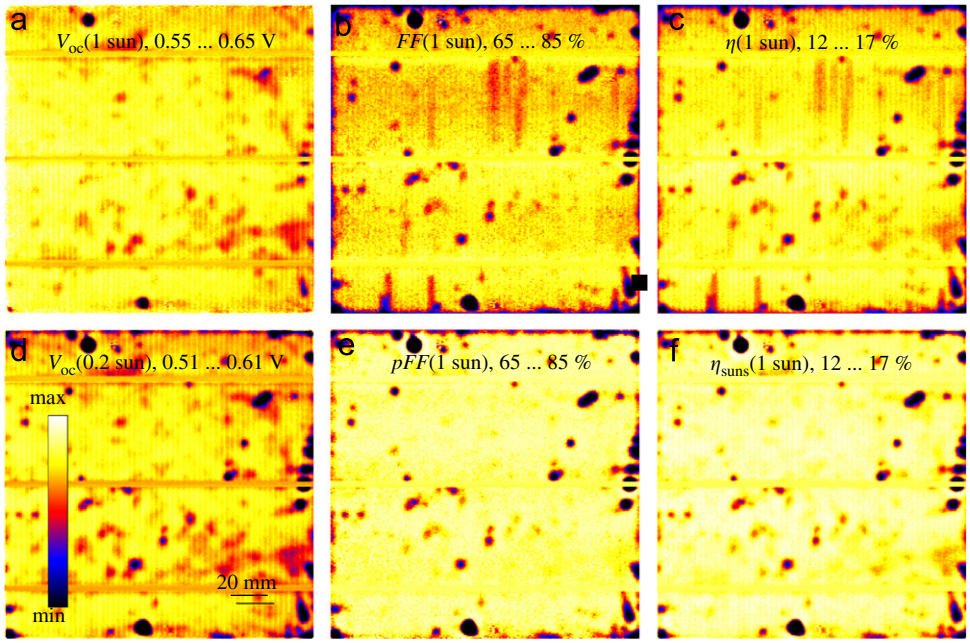

Fig. 5. (a) V_{oc} at 1 sun, (b) FF at 1 sun, (c) efficiency at 1 sun, (d) V_{oc} at 0.2 sun, (e) "suns-V_{oc}" pseudo-FF at 1 sun, (f) "suns-V_{oc}" efficiency at 1 sun. All scaling ranges are indicated, the color and scaling bars in (d) hold for all images.

A valuable feature of "Local I–V 2" is that it allows one to consider single pixels or certain (rectangular) local regions as "bad pixel" regions. Then all input data in these regions are automatically replaced by the average data of their surrounding. This feature may also be applied to replace the data from the bus bar region, where no useful DLIT and EL signals appear, by more meaningful data of the surrounding. Another related feature is the "cut shunt" option. Here a shunt region may be selected and all input data of this region are replaced by average data of its surrounding. However, in contrast to the "bad pixel" option, here the total cell current values are corrected according to the local current data in the selected region. Now this option will be used to check the influence of the two dominant shunts at the top and at the bottom of the cell on the efficiency of the whole cell at different illumination intensities. For the whole cell, the efficiency at one sun intensity was calculated to be 15.48%, and at 0.2 suns it was 13.78%. After having cut out these two shunts, at one sun intensity the expected efficiency is 15.57% and at 0.2 suns it is

14.04%. This shows that, though these shunts are dominating the DLIT images, their influence on the efficiency at one sun is with 0.085% (absolute) relatively small. However, at 0.2 suns illumination intensity these shunts degrade the efficiency already by 0.26% (absolute), which is not negligible anymore. This could be expected since, according to Fig. 1c, 3a, 3c, and 3f, these shunts contain only ohmic and J_{02}-contributions with a large ideality factor, but no J_{01}-contribution.

4. Discussion

It has been mentioned already in the Sect. 2 that the "Local *I–V* 2" procedure is based on a number of relatively strong assumptions. Thus, this procedure is only of limited accuracy and cannot replace a rigorous 2-D or 3-D device simulation. However, as a rule such device simulations are assuming homogeneous silicon material and do neither consider local lifetime variations nor any technological imperfections like scratches or grid line interruptions. The strength of the procedure described here is that it may evaluate real solar cells showing such inhomogeneities nondestructively. It was already mentioned in Sect. 1 that the local cell parameter images are actually only hypothetical ones, which would hold if a whole homogeneous cell would show the properties of a certain region. Thus, it is not allowed to average these parameters over a certain region. However, the influence of a certain local defect may be evaluated quantitatively by simulating illuminated *I–V* characteristics of a representative region of the cell containing this defect or not and comparing these parameters with the parameters simulated for the whole cell. At least, the local cell parameter images simulated by "Local *I–V* 2" enable a qualitative estimation, which defects are most detrimental e.g., for degrading the *FF* or V_{oc}, how the series resistance influences the efficiency, and how these influences changes with varying illumination intensity. The demonstrated very good correspondence between measured cell parameters and parameters simulated for the whole cell, based on local DLIT and EL images, indicates that this procedure works sufficiently realistic on typical industrial solar cells.

It would be interesting to compare this method with the ILIT-based local efficiency analysis of Ramspeck et al. [14] and with the PL-based analysis recently introduced by Shen et al. [15], as well as with the PL-based local efficiency analysis working on wafers, which was recently introduced by Michl et al. [23] Thus, it can be expected that the DLIT-based local efficiency analysis introduced here, which is available via [16], will become a useful tool for the PV community.

Acknowledgement

The author is grateful to D. Hinken (ISFH Hamelin) for providing the PL-R_s data used here, to S. Rißland (MPI Halle) for performing DLIT and *I–V* characteristics measurements, and to K. Iwig (MSC-Technik Halle) for writing the "Local *I–V* 2" code. This work was financially supported by the German Federal Ministry for the Environment, Nature Conservation and Nuclear Safety and by industry partners within the research cluster "SolarWinS" (contract No. 0325270C). The content is the responsibility of the author.

Refrences

[1] O. Breitenstein, W. Eberhardt, K. Iwig, Imaging the local forward current density of solar cells by dynamical precision contact thermography, Proc. 1st World Conf. on Photovolt. Energy Conv., Hawaii 1994, pp. 1633–1636.
[2] O. Breitenstein, K. Iwig, I. Konovalov, Evaluation of local electrical parameters of solar cells by dynamic (lock-in) thermography, Physica Status Solidi (a) 160 (1997) 271–282.
[3] O. Breitenstein, W. Warta, M. Langenkamp, Lock-in Thermography—Basics and Use for Evaluating Electronic Devices and Materials, second ed., Springer, Berlin/Heidelberg, 2010.
[4] S.M. Sze, K.K. Ng, Physics of Semiconductor Devices, third ed., Wiley, Hoboken NJ, 2007, pp. 90–98.
[5] D. Macdonald, A. Cuevas, Reduced fill factors in multicrystalline silicon solar cells due to injection-level dependent bulk recombination lifetimes, Progress in Photovoltaics: Research and Applications 8 (2000) 363–375.
[6] S. Steingrube, O. Breitenstein, K. Ramspeck, S. Glunz, A. Schenk, P.P. Altermatt, Explanation of commonly observed shunt currents in C–Si solar cells by means of recombination statistics beyond the Shockley-Read-Hall approximation, Journal of Applied Physics 110 (2011) 014515.
[7] O. Breitenstein, M. Langenkamp, Quantitative local analysis of *I–V* characteristics of solar cells by thermal methods, Proc. 2nd World Conf. on Photovolt. Energy Conv., Vienna 1998, pp. 1382–1385.
[8] O. Breitenstein, Nondestructive local analysis of current–voltage characteristics of solar cells by lock-in thermography, Solar Energy Materials & Solar Cells 95 (2011) 2933–2936.
[9] T. Trupke, E. Pink, R.A. Bardos, M.D. Abbott, Spatially resolved series resistance of silicon solar cells obtained from luminescence imaging, Applied Physics Letters 90 (2007) 093506.
[10] J. Haunschild, M. Glatthaar, M. Kasemann, S. Rein, E.R. Weber, Fast series resistance imaging for silicon solar cells using electroluminescence, Physica Status Solidi (RRL) 4 (2009) 227–229.
[11] K. Ramspeck, K. Bothe, D. Hinken, B. Fischer, J. Schmidt, R. Brendel, Recombination current and series resistance imaging of solar cells by combined luminescence and lock-in thermography, Applied Physics Letters 90 (2007) 153502.
[12] R. Sinton, A. Cuevas, A quasi-steady-state open-circuit voltage method for solar cell characterization, Proc. 16th Eur. Photovolt. Solar Energy Conf., Glasgow 2000, pp. 1152–1155.
[13] W. Warta, J. Sutter, B. Wagner, and R. Schindler, Proc. Second World Conf. on Photovolt. Energy Conv., Vienna, Austria, 1998, pp. 1650–1653.
[14] K. Ramspeck, K. Bothe, J. Schmidt, R. Brendel, Correlation between spatially resolved solar cell efficiency and carrier lifetime of multicrystalline silicon, Journal of Materials Science: Materials in Electronics 19 (2008) S4–S8.
[15] C. Shen, H. Kampwerth, M. Green, Spatially resolved photoluminescence imaging of essential silicon solar cell parameters, oral contribution at 38th IEEE Photovoltaic Specialists Conference, Austin TX 2012, proceedings in print.
[16] 〈http://max-planck-innovation.de/en/〉.
[17] S.R. Robinson, A.G. Aberle, M.A. Green, Departures from the principle of superposition in silicon solar cells, Journal of Applied Physics 76 (1994) 7920–7930.
[18] G.L. Araújo, A. Cuevas, J.M. Ruiz, The effect of distributed series resistance on the dark and illuminated current–voltage characteristics of solar cells, IEEE Transactions on Electron Devices 33 (1986) 391–401.
[19] O. Breitenstein, J.P. Rakotoniaina, Electrothermal simulation of a defect in a solar cell, Journal of Applied Physics 97 (2005) 074905.
[20] H. Straube, J.-M. Wagner, O. Breitenstein, Measurement of the Peltier coefficients of semiconductors by lock-in thermography, Applied Physics Letters 95 (2009) 052107.
[21] O. Breitenstein, J. Bauer, K. Bothe, D. Hinken, J. Müller, W. Kwapil, M.C. Schubert, W. Warta, Can luminescence imaging replace lock-in thermography on solar cells? IEEE Journal of Photovoltaics 1 (2011) 159–167.
[22] O. Breitenstein, A. Khanna, Y. Augarten, J. Bauer, J.-M. Wagner, K. Iwig, Quantitative evaluation of electroluminescence images of solar cells, Physica Status Solidi (RRL) 4 (2010) 7–9.
[23] B. Michl, M. Rüdiger, J.A. Giesecke, M. Hermle, W. Warta, M.C. Schubert, Efficiency limiting bulk recombination in multicrystalline silicon solar cells, Solar Energy Materials & Solar Cells 98 (2012) 441–447.